Journal of
Mechanics of
Materials and Structures

SLIP DAMPING OF A PRESS-FIT JOINT UNDER NONUNIFORM PRESSURE DISTRIBUTION ALONG THE INTERFACE

Huifang Xiao, Yunyun Sun and Jinwu Xu

Volume 15, No. 3 May 2020

msp

JOURNAL OF MECHANICS OF MATERIALS AND STRUCTURES
Vol. 15, No. 3, 2020
https://doi.org/10.2140/jomms.2020.15.307

SLIP DAMPING OF A PRESS-FIT JOINT UNDER NONUNIFORM PRESSURE DISTRIBUTION ALONG THE INTERFACE

HUIFANG XIAO, YUNYUN SUN AND JINWU XU

The energy dissipation and the damping capacity of a press-fit joint under a vertical load are investigated using the continuum elastic beam model. The clamping pressure is considered to be of power law with distance along the contact interface and the corresponding relative displacements under vertical load are derived. Expression of the minimum critical vertical load inducing relative slip along the contact interface is determined. The hysteresis curves of the vertical forces as a function of the relative displacement at the contact interface are obtained for different pressure distribution laws and the associated energy dissipations are presented. The damping ratio of the assembled structure is further evaluated. It is shown that peak values of damping ratio exist for different pressure distribution laws and the normal load at which the peak damping ratio occurs is a function of the pressure distribution law. Three-dimensional finite element analysis validation is performed, which shows good agreement with model predictions.

1. Introduction

Bolted joints are indispensable in build-up machine and mechanical devices with different structure members assembled together, which provide coupling forces and moments between structures. The local relative slip occurring along the frictional joint interface contribute significantly to the damping mechanism of the structure and therefore plays an important role in the dynamic performance and fatigue life of the system [Berger 2002; Ahmadian and Jalali 2007; Yokoyama et al. 2012; Hammami et al. 2016; Choi et al. 2018].

Due to its significance, great effort has been expended on the relative microslip motion at the jointed contact interface as well as the associated energy dissipation and damping capability. As for the modeling of joint behavior, two kinds of models as discrete model and continuum model are developed to represent the microslip motion along the frictional interface in the mechanical joints. The basic discrete model of the frictional interface was developed in [Iwan 1966]. In the Iwan models, the microslip motions are characterized using reduced-order distributed-parameter models. Based on the Iwan model, different discrete models [Song et al. 2004; Segalman 2005; Miller and Quinn 2009; Li et al. 2017] were developed to capture different contact behaviors at the joint interface. As for the continuum models of the microslip motion in joints, the frictional interface is generally described using one-dimensional elastic beam with or without a shear layer between the beam and the frictional ground [Menq et al. 1986; Csaba 1998; Cigeroglu et al. 2006; Asadi et al. 2012].

The effects that related to the contact properties of the interacting surfaces will exhibit influence on the relative motion as well as the energy dissipation and damping capacity of the jointed assembly. These effects have also been studied widely by experiment methods or finite element (FE) simulations. Nanda

Keywords: press-fit joint, nonuniform pressure distribution, energy dissipation, damping ratio.

[2006] experimentally studied the effect of interfacial pressure intensity, diameter of the connecting bolts, number of layers, kinematic coefficient of friction as well as frequency and amplitude of excitation on the damping capacity of layered and jointed structure. The results show that the interfacial pressure intensity and number of layers play a major role on the damping capacity of the jointed structure. Daouk et al. [2017] investigated the effect of shear loading level on the energy dissipation of bolted joint through the model testing of a designed dynamic test rig based on a bolted structure. Stocchi et al. [2013] established a single lap composite bolted joint with countersunk fasteners under static shear tensile load and studied the influence of bolt clamping force, coefficient of friction and bolt-hole clearance on the joint behavior. Chen and Deng [2005] studied the frictional damping at joint interfaces under uniform pressure distribution using the finite element method. Thai and Uy [2015] developed a three-dimensional finite element model to study the effects of column sections and different types of blind bolts on the five motion stages of no slip, slip, full contact, damage and final failure of blind bolted endplate composite joints. Abad et al. [2014] performed both experimental tests and finite element simulations on a bolted lap joint to obtain the force-displacement relationship and to assess the effects of preload on the stick-slip regime between the bolted plates. The parameters of the Valanis model, describing the frictional behavior at the interface are also obtained using the calculated hysteresis cycles.

These previous studies were mostly restricted to the assumption of uniform pressure distribution at the interface, which can be only achieved in condition that the space between consecutive connecting bolts is about two times the diameter of the connecting bolts [Gould and Mikic 1972; Marshall et al. 2006]. The effect of nonuniform pressure distribution at the interface on the contact behavior has also received attention. Cigeroglu et al. [2006] presented a one-dimensional beam model to analyze the stick-slip transitions along the interface under convex and concave nonuniform pressure distributions. Xiao et al. [2014] investigated the energy dissipation in a shear lap joint by considering the effect of interface tangential contact stiffness and nonuniform pressure distribution at the interface. However, the models and results are limited to shear lap joints subjected to tangential load along the interface, which is different from the press-fit joints subjected to a vertical load.

The present work is the extension of the pervious study from shear lap joint to press-fit joint subjected to nonuniform pressure distribution along the interface and a vertical load at the free end. The variation of clamping pressure is assumed to be of exponent law with distance along the contact interface and the corresponding relative displacements under vertical load are derived using the continuum elastic beam model. The hysteresis curves of the vertical forces as a function of the relative displacement at the contact interface are obtained for different pressure distribution laws and the associated energy dissipations are presented. The damping ratio is further evaluated and compared with the finite element modeling results.

2. Description of the studied model

The schematic diagram of a press-fit joint under a vertical force at the free end is shown in Figure 1, left. Two rectangular beams with identical dimensions and material properties are bolt jointed under the clamping force F_n. The dimensions of the beams are length $2L$, height h, width b and the diameter of the bolt is $2R$. The resulted pressure distribution along the interface is parabolic and the influence zone is a circle with 3.5 times the diameter of the connecting bolt [Gould and Mikic 1972; Marshall et al. 2006], i.e., $L = 3.5R$, as shown in Figure 1, right.

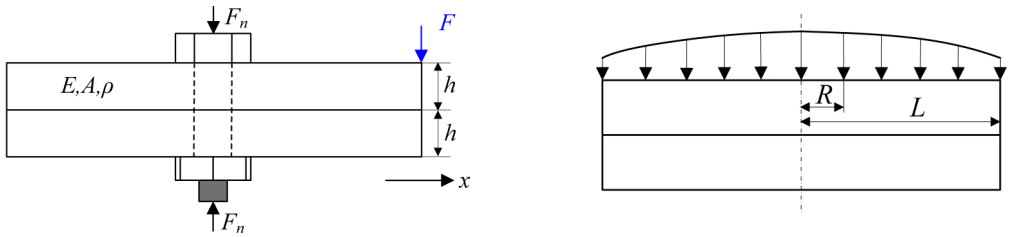

Figure 1. Left: schematic diagram of a press-fit joint under a vertical force at the free end. Right: pressure distribution along the interface.

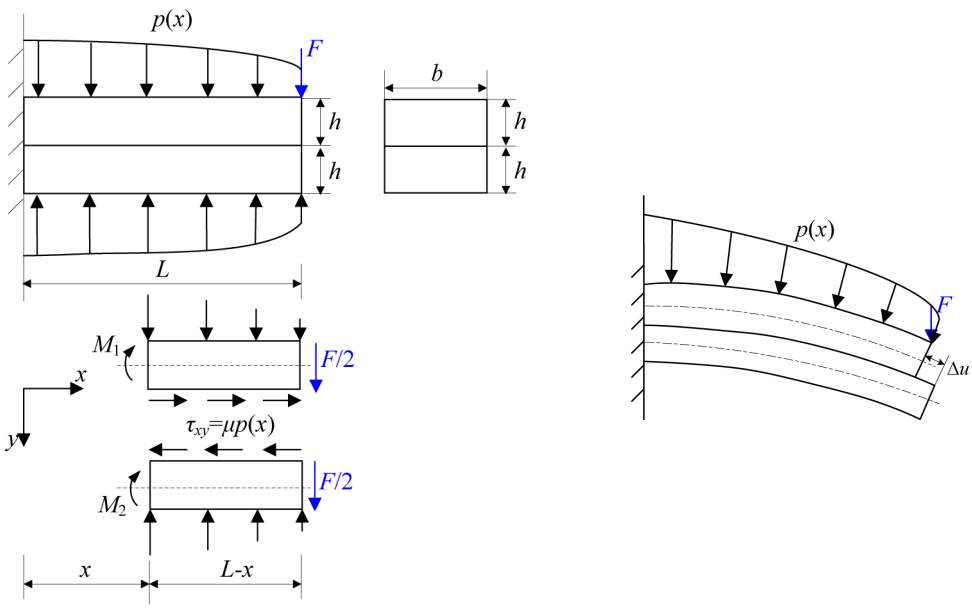

Figure 2. Left: model for examining the relative slip motion at the joint interface and the free-body diagram of the beams. Right: relative motion at the frictional interface under the vertical load, with u the relative displacement at the joint interface.

Figure 2, left, shows the model for examining the relative slip motion at the interface. The left end of the layered jointed beams is fixed. A vertical force F is applied at the right end of the beams. The friction law at the joint interface is represented using the Coulomb model with a constant friction coefficient μ. The relative slip motion at the frictional interface is induced by the vertical force F and is also influenced by the pressure distribution characteristics, as shown in Figure 2, right.

It is assumed that the interfacial pressure along the interface is of exponent law function and can be expressed as follows [Xiao et al. 2014]:

$$p(x) = p_0\left(1 - \frac{1}{2}\left(\frac{x}{L}\right)^{\alpha}\right), \tag{1}$$

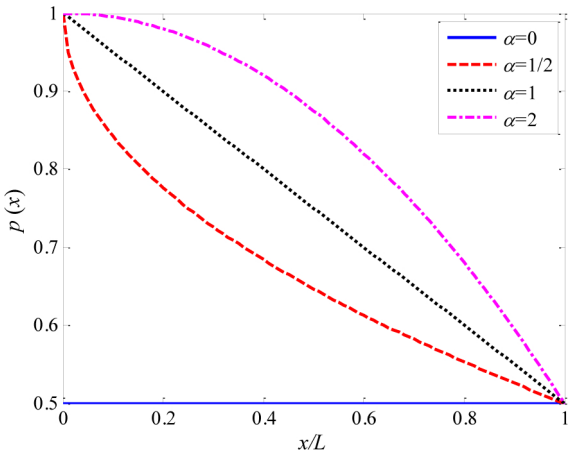

Figure 3. Pressure distributions along the interface for different laws with $p_0 = 1$.

where p_0 is the amplitude of pressure, α is the coefficient denoting different pressure laws, i.e., $\alpha \geq 0$. Figure 3, shows the profiles of pressure distributions for different laws.

3. Relative slip responses

According to the free-body diagram in Figure 2, left, the governing equation for the layered beams in bending can be expressed as

$$EI\frac{d^2w}{dx^2} - \frac{F}{2}(L-x) + \mu p(x)(L-x)b\frac{h}{2} = 0 \tag{2}$$

and the boundary conditions can be found as

$$(dw/dx)_{x=0} = 0, \quad w(0) = 0, \tag{3}$$

where $w(x)$ is the vertical deflection at point x, E is the Young's modulus, I is the moment of inertia of the beam. The solution for vertical deflection can be obtained as

$$w(x) = \frac{(F-\mu p_0 bh)L^3}{Ebh^3}\left[3\left(\frac{x}{L}\right)^2 - \left(\frac{x}{L}\right)^3\right] + \frac{3\mu p_0 L^3}{Eh^2(\alpha+2)}\left[\frac{1}{\alpha+1}\left(\frac{x}{L}\right)^{\alpha+2} - \frac{1}{\alpha+3}\left(\frac{x}{L}\right)^{\alpha+3}\right]. \tag{4}$$

We introduce nondimensional parameters for position, normal load and vertical deflection:

$$\bar{x} = \frac{x}{L}, \quad \bar{F} = \frac{F}{\mu p_0 bh}, \quad \bar{w} = \frac{w}{\mu p_0 L^3/Eh^2}.$$

The nondimensional vertical deflection can be written as

$$\bar{w}(\bar{x}) = (\bar{F}-1)(3\bar{x}^2 - \bar{x}^3) + \frac{3}{\alpha+2}\left[\frac{1}{\alpha+1}\bar{x}^{\alpha+2} - \frac{1}{\alpha+3}\bar{x}^{\alpha+3}\right]. \tag{5}$$

Figure 4 shows the nondimensional vertical deflection along the beam length for different pressure distribution laws with $\alpha = 0, \frac{1}{2}, 1, 2$. The nondimensional normal load used in calculation is $\bar{F} = 3$. It can be seen that the vertical deflection increases along the beam length from $\bar{w} = 0$ at the fixed end to the

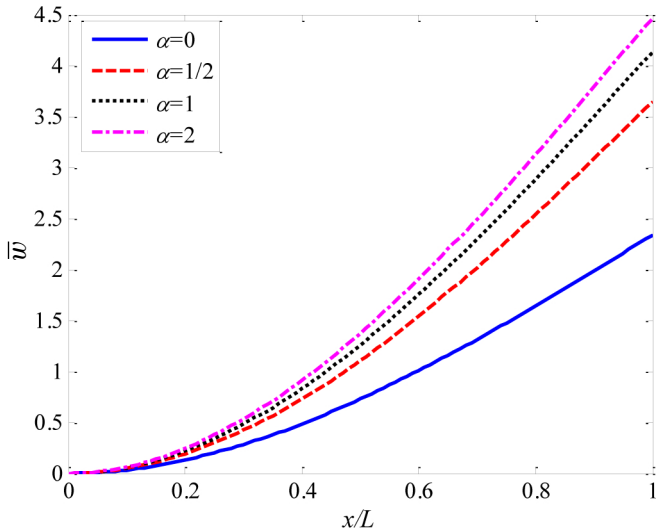

Figure 4. Nondimensional vertical deflection along the beam length for different pressure distribution laws. The nondimensional normal load used in calculation is $\bar{F} = 3$.

maximum at free end where the load is applied. The pressure distribution laws show significant effect on the vertical deflection. The vertical deflection under a uniform pressure distribution with $\alpha = 0$, is smaller than that of the nonuniform pressure distributions at the same position. The nonuniform pressure distribution $\alpha = 2$ has the maximum value of deflection.

3.1. ***Relative slip displacement.*** The relative dynamic slip at the contact interface is given by [Masuko et al. 1973]

$$u(x) = u_2(x) - u_1(x), \tag{6}$$

where $u_1(x)$ and $u_2(x)$ are the displacements at position x on opposite sides of the interface. The displacements are related to the in-plane bending stress and moment about the centroid of each half of the beam as

$$\begin{aligned} u_1(x) &= \frac{1}{E}\int_0^x \frac{\mu p(x)(L-x)}{h}dx - \frac{h}{2}\frac{dw_1}{dx}, \\ u_2(x) &= \frac{1}{E}\int_0^x -\frac{\mu p(x)(L-x)}{h}dx + \frac{h}{2}\frac{dw_2}{dx}. \end{aligned} \tag{7}$$

Assuming the vertical deflection is continuous across the section, i.e., $w_1(x) = w_2(x) = w(x)$, and combining (1), (4), (6) and (7), the relative slip can be expressed as

$$u(x) = \frac{(3F - 5\mu p_0 bh)L^2}{Ebh^2}\left[2\left(\frac{x}{L}\right) - \left(\frac{x}{L}\right)^2\right] - \frac{5\mu p_0 L^2}{Eh}\left[\frac{1}{(\alpha+2)}\left(\frac{x}{L}\right)^{\alpha+2} - \frac{1}{(\alpha+1)}\left(\frac{x}{L}\right)^{\alpha+1}\right]. \tag{8}$$

Introducing the nondimensional parameter $\bar{u} = u/[\mu p_0 L^2/(Eh)]$, the nondimensional relative slip can be written as

$$u'(\bar{x}) = (3\bar{F} - 5)(2\bar{x} - \bar{x}^2) - 5\left[\frac{1}{\alpha+2}\bar{x}^{\alpha+2} - \frac{1}{\alpha+1}\bar{x}^{\alpha+1}\right]. \tag{9}$$

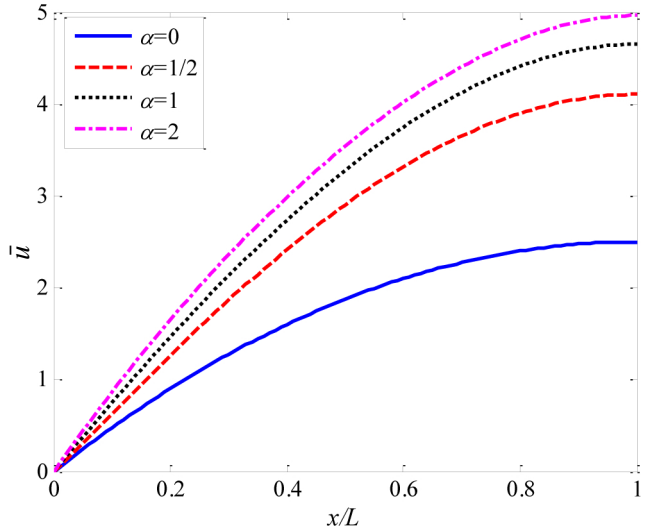

Figure 5. Nondimensional relative slip along the beam length for different pressure distribution laws. The nondimensional normal load $\overline{F} = 3$.

Figure 5 shows the nondimensional relative slip along the beam length for different pressure distribution laws with $\alpha = 0, \frac{1}{2}, 1, 2$. It can be seen that the relative slip also increases along the beam length from $\overline{w} = 0$ at the fixed end to the maximum at free end, similar as that for the vertical deflection. Effect of pressure distribution laws on the relative slip is obvious. The relative slip under a uniform pressure distribution with $\alpha = 0$, is smaller than that of the nonuniform pressure distributions at the same position. The relative slip increases with increasing pressure law value α.

3.2. ***Energy dissipation.*** The energy dissipation per cycle at the frictional interface is expressed as [Xiao et al. 2014]

$$E_d = 4b \int_0^L \mu p(x) u(x)\, dx. \tag{10}$$

Substituting the pressure distribution law (1) and the relative slip displacement expression (8) into (10), the energy dissipation can be obtained as

$$E_d = \frac{4\mu p_0 (3F - 5\mu p_0 bh) L^2}{Eh^2} C_1 - \frac{20(\mu p_0 L)^2 b}{Eh} C_2, \tag{11}$$

where

$$C_1 = \frac{2}{3} - \frac{1}{\alpha+2} + \frac{1}{2(\alpha+3)}, \quad C_2 = \frac{1}{(\alpha+2)(\alpha+3)} - \frac{1}{(\alpha+1)(\alpha+2)} - \frac{1}{2(\alpha+2)(2\alpha+3)} + \frac{1}{4(\alpha+1)^2}.$$

Introducing the nondimensional parameter $E_f = \dfrac{E_d}{(\mu p_0 L)^2 b/(Eh)}$, we can express the nondimensional energy dissipation per cycle as

$$E_f = (12\overline{F} - 20)C_1 - 20C_2. \tag{12}$$

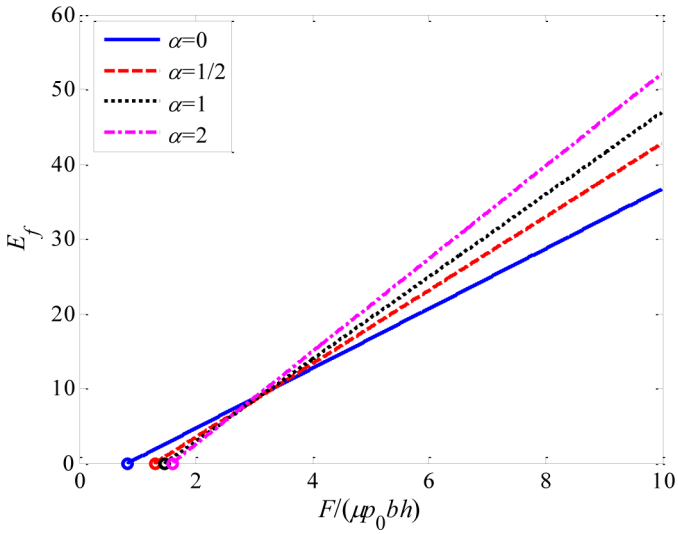

Figure 6. Nondimensional energy dissipation as a function of nondimensional normal load for different pressure distribution laws. The symbols ◯ is for the minimum force values inducing relative slip.

It is noted that the energy dissipation has $E_f > 0$ when relative slip occurs. Accordingly, the minimum force to induce the relative slip at the contact interface is determined as

$$\overline{F}_{\min} = \frac{5}{3}\left(1 + \frac{C_2}{C_1}\right). \tag{13}$$

It can be seen that the minimum force to induce the relative slip is only a function of the pressure distribution law.

Figure 6 shows the normalized energy dissipation per cycle, E_f, versus the normal load $F/(\mu p_0 bh)$ for the four different pressure distribution laws. As can be seen, effect of pressure distribution law on the energy dissipation is obvious and depends on the applied normal load. For small normal load, i.e., $F/(\mu p_0 bh) < 3$, the largest energy dissipation occurs at the uniform pressure distribution for the same normal load; whilst the nonuniform pressure distribution $\alpha = 2$ has the minimum value. However, as the normal load increases, i.e., $F/(\mu p_0 bh) > 3$, the largest energy dissipation occurs with $\alpha = 2$; whilst the uniform pressure distribution has the minimum energy dissipation The increasing rate of energy dissipation with normal load increases with pressure law value α, i.e., the slop of the curve increases for the same normal load with increasing α value.

Figure 7 shows the variation of the minimum normal load inducing relative slip motion at the contact interface with pressure distribution law. The minimum normal load exhibits a quick increase with pressure distribution law for small value of α, i.e., $\alpha < 2$. As the law value becomes larger, the minimum normal load almost keeps the same value of $F_{min} = 1.65$ and not varying with pressure distribution law values.

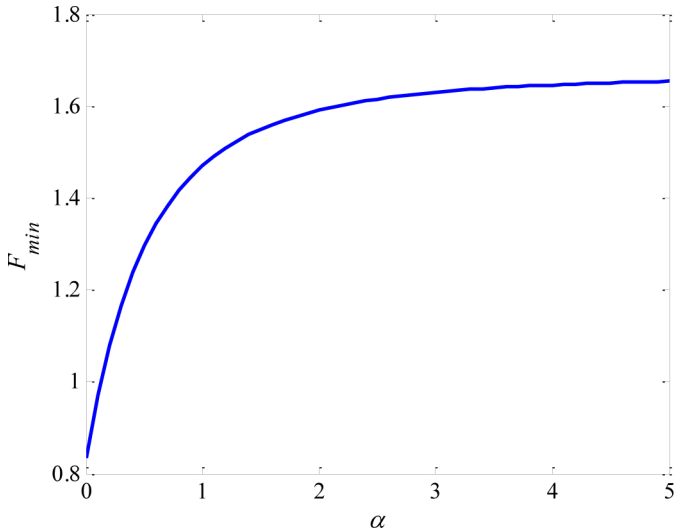

Figure 7. Variation of the minimum nondimensional normal load for relative slipping occurring as a function of pressure distribution law.

3.3. ***Hysteresis curves.*** The vertical deflection at the right end of the beam where the load is applied, $W = \overline{w}(1)$, can be obtained from (5) by setting $\bar{x} = 1$ as

$$W = \overline{w}(1) = 2(\overline{F} - 1) + \frac{3}{(\alpha+2)}\left(\frac{1}{\alpha+1} - \frac{1}{\alpha+3}\right). \tag{14}$$

Equation (14) is the monotonic loading force-deflection relationship at the free end for the layered beams, which illustrates a linear relationship between force and deflection with a constant stiffness value of $\frac{1}{2}$. To determine the whole hysteresis loop under the cyclic vertical load, it is necessary to compute the force-deflection relationship for the unloading and reloading process. It is noted that relative slip can be only initiated when the applied load reaches the minimum load F_{min} in (13). For load smaller than F_{min}, no relative slip occurs at the interface and the beams are in elastic deflection regime with the elastic stiffness has the expression of

$$k_1 = \frac{\overline{F}_{\min}}{W_{\min}} = \frac{\overline{F}_{\min}}{2(\overline{F}_{\min} - 1) + \frac{3}{(\alpha+2)}\left(\frac{1}{\alpha+1} - \frac{1}{\alpha+3}\right)}. \tag{15}$$

Equation (15) shows that the stiffness, i.e., slope of the force-deflection relationship in elastic deflection regime is dependent on the pressure distribution law. The unloading process follows the same elastic deflection regime with stiffness k_1. Accordingly, the force-deflection relationship in the unloading and reloading process can be determined as

$$F_u = k_1(W_u - W^*) - F^*, \tag{16}$$

$$F_r = k_2(W_r + W^*) - F^*, \tag{17}$$

where F_u and F_r are the unloading and reloading force respectively, F^* and W^* are the force and displacement values at which the loading process reversed, k_2 is the slope of the loading force-deflection

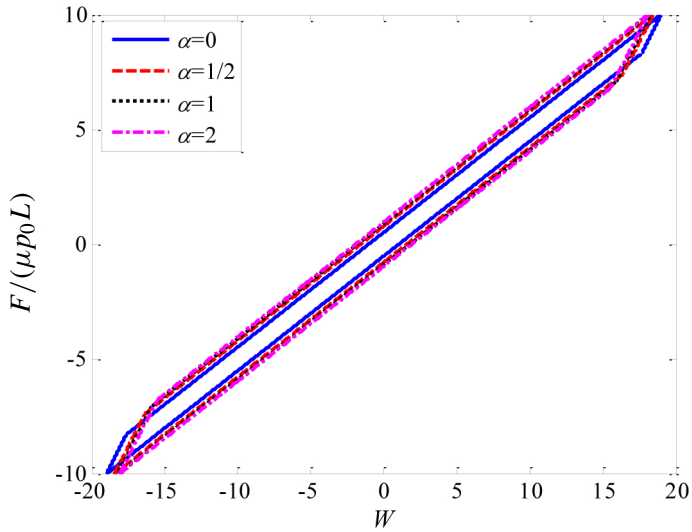

Figure 8. Effect of pressure distribution laws on the hysteresis loop.

relationship, i.e., $k_2 = \frac{1}{2}$, W_u and W_r are the unloading and reloading displacement, respectively. The reloading displacement, W_r, is the negative of the unloading displacement with a negative argument

$$W_r = -W_u. \tag{18}$$

It is clear from (15), (16) and (17) that the properties of the hysteresis loop are embedded in the first loading curve and the minimum load initiating the relative slip

Figure 8 shows the hysteresis curves for different pressure distribution laws. In order to illustrate the effect of pressure distribution laws, the load reversals are chosen to be identical as $F^* = 10$. It can be seen that the pressure distribution law significantly affects the area of the hysteresis cycle and the corresponding value of energy dissipated. The slopes of the force-deflection relationship in the loading and reloading process are constant with $k_2 = \frac{1}{2}$ and are identical for different pressure distribution laws. Although the slope of the force-deflection relationship in the unloading process, i.e., k_1 depends on the pressure distribution law α, the variation of k_1 with α is very slight, as shown in Figure 9. The slope k_1 can be also regarded as constant value. Consequently, the force-deflection curves in the unloading process for different pressure distribution laws are also parallel with almost identical stiffness values.

3.4. ***Damping ratio.*** The damping capacity of the layered beam structure can be characterized using the damping ratio

$$\zeta = \frac{\delta}{\sqrt{(2\pi)^2 + \delta^2}} \approx \frac{\delta}{2\pi}, \tag{19}$$

where δ is the logarithmic damping coefficient and is related to the energy dissipation from two consecutive cycles as follows:

$$\delta = \frac{1}{2} \ln\left(1 + \frac{E_d}{E_{ne}}\right), \tag{20}$$

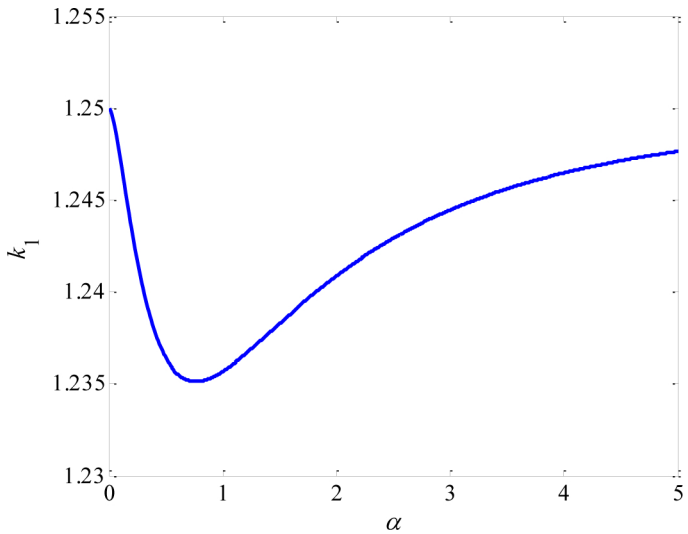

Figure 9. Variation of the slope for force-deflection relationship in the unloading process.

where E_d is the energy loss per cycle, E_{ne} is the maximum

$$E_{ne} = \frac{3}{2}\frac{EI}{L^4}w^2(L), \tag{21}$$

where $I = 2bh^3/3$ is the moment of inertia of the clamped layered beam, $w(L)$ is the vertical deflection at the free end where the load is applied and can be obtained using (4). Accordingly, the strain energy can be determined as

$$E_{ne} = \frac{4bL^2}{Eh}\left[\frac{F-\mu p_0 bh}{bh} + \frac{3\mu p_0}{(\alpha+1)(\alpha+2)(\alpha+3)}\right]^2. \tag{22}$$

Combining (19), (20), (11) and (22), the damping ratio of the layered beams can be determined.

Figure 10 shows the relationship between damping ratio and nondimensional normal load $F/(\mu p_0 bh)$ for different pressure distribution laws with $\alpha = 0, \frac{1}{2}, 1, 2$. Effect of pressure distribution law on the energy dissipation is obvious and this effect is also depends on the applied normal load. For small normal load, the value of damping ratio increases with applied normal load and the largest damping ratio occurs for the uniform pressure distribution with $\alpha = 0$, and the minimum damping ratio is obtained for the pressure distribution with pressure distribution law $\alpha = 2$. As the normal load increases, the value of damping ratio decreases and the largest damping ratio occurs for the pressure distribution with pressure distribution law $\alpha = 2$, and the minimum damping ratio is obtained for uniform pressure distribution. The peak values of damping ratio exist for different pressure distribution laws.

The normal load at which the peak damping ratio occurs can be determined by

$$\frac{d\zeta}{d\bar{F}} = 0. \tag{23}$$

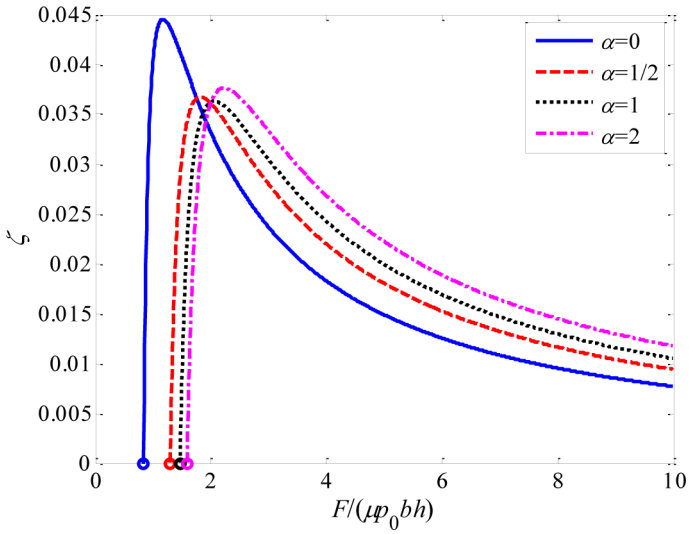

Figure 10. Plots of the relationship between damping ratio and nondimensional normal load for different pressure distribution laws. The symbol ◯ denotes the minimum force values inducing relative slip.

The corresponding normal load is determined as

$$F_0 = \frac{10C_2}{3C_1} + \frac{10}{3} + C_3 - 1, \tag{24}$$

where

$$C_3 = \frac{3}{(\alpha+1)(\alpha+2)(\alpha+3)}.$$

Figure 11 shows the dependence of the normal load at which the peak damping ratio occurring, F_0, on the pressure distribution law. It can be seen that the variation of normal load F_0 with law α shows similar behavior as that for the minimum normal load inducing relative slip motion, as shown in Figure 6. The value of F_0 exhibits a quick increase with pressure distribution law for small value of α, i.e., $\alpha < 2$. As the law value becomes larger, the peak damping ratio normal load almost keeps the same value of $F_0 = 2.25$ and not varying with pressure distribution laws.

4. Comparison with finite element modeling

In order to validate the developed model for slip damping calculation, the layered cantilever beam model as shown in Figure 2, left, is further studied using 3D dynamic finite element analysis (FEA) to determine the damping ratio at the interface. The calculated values of damping ratio using FEA are compared with that using the developed model of (19)–(22) for four different pressure distribution laws of uniform pressure distribution with $\alpha = 0$ and nonuniform pressure distribution with $\alpha = \frac{1}{2}$, 1, 2.

The half-power bandwidth method [Ewins 2000] is employed to determine the damping ratio of the layered cantilever beam model for FEA results. In this method, the frequency response function (FRF) of the system is obtained firstly. Figure 12 shows the schematic diagram of the frequency response function.

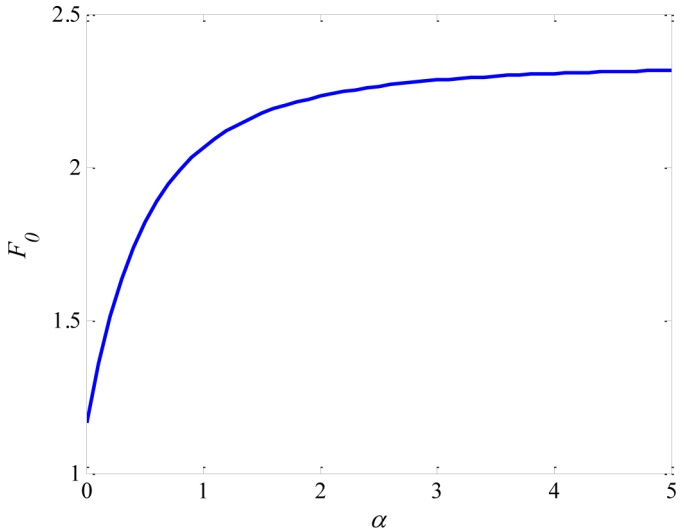

Figure 11. Plot of the variation of the normal load at which the peak damping ratio occurring with the pressure distribution law.

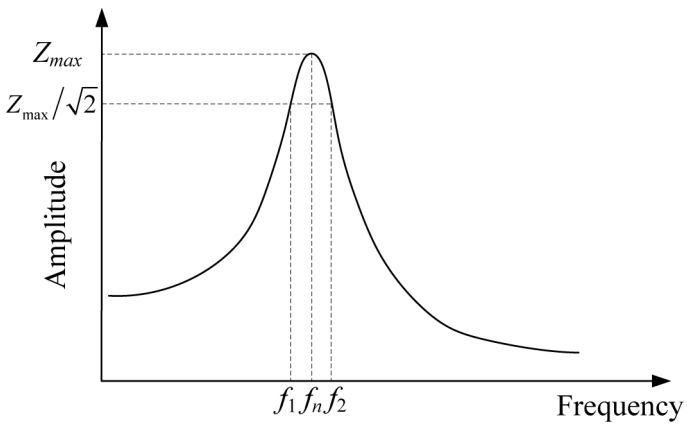

Figure 12. Half-power bandwidth method for estimation of the damping ratio.

The maximum displacement at resonance is $Z_{\max}$ and the corresponding resonant frequency is f_n. The half-power points are determined at which the amplitudes are $Z_{\max}/\sqrt{2}$ and the corresponding frequencies are f_1 and f_2, located on either side of the resonant frequency. The damping ratio is evaluated as

$$\zeta = \frac{f_2 - f_1}{2f_n}, \tag{25}$$

where f_n is the resonant frequency, f_1 and f_2 are the half-power points at which the amplitude is $Z_{\max}/\sqrt{2}$, $Z_{\max}$ is the amplitude at resonance.

In order to obtain the frequency response function (FRF) of the system, the layered cantilever beams are excited at the free end with an impulse excitation. The impulse has the rectangular shape shown in

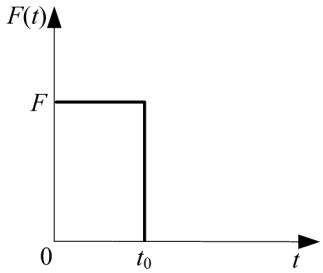

Figure 13. Rectangular impulse force applied at the free end of the beams.

Figure 13 and is modeled as

$$\begin{aligned} F(t) &= F, \quad 0 \le t \le t_0, \qquad (26) \\ F(t) &= 0, \qquad t > t_0, \qquad (27) \end{aligned} \tag{28}$$

where F and t_0 are the amplitude and duration of the impulse excitation.

The output vibration signals on the other side at the free end of the beam are collected. The frequency response function (FRF) of the system can be calculated by dividing the acceleration responses of the beam with respect to the impulse excitation in frequency domain. The damping ratio can be then evaluated from the frequency spectrum.

Figure 14 shows the finite element mesh for the layered cantilever beam model. The dimensions of the beams are 300 mm×50 mm×8 mm. The beams are discretized using element SOLID185. The contact interaction at the frictional interface is modeled using surface-to-surface contact and calculated using the penalty method [Zhong 1993]. The mesh convergence is obtained by iteratively increasing the mesh density until the responses differed by less than 1% between iterations [Xiao et al. 2012]. The nodes at the left hand side of the beams were constrained from moving in all directions. A rectangle pulse with time duration of $t_0 = 1 \times 10^{-5}$s is applied on the upper surface of the assembly at the free end. The responses at the bottom surface of the assembly at the free end are collected. Four different pressure distributions with amplitude p_0=1 MPa and law $\alpha = 0$, $\frac{1}{2}$, 1 and 2 are applied on the upper surface of the beam, respectively. The time step employed in the calculations is 1×10^{-5} s.

In order to examine the accuracy of the finite element model, the static analysis of the layered cantilever beam model with a static vertical force at the free end is performed firstly. The amplitude of the vertical force is F=160N. The vertical deflection and relative slip along the beam length for different pressure

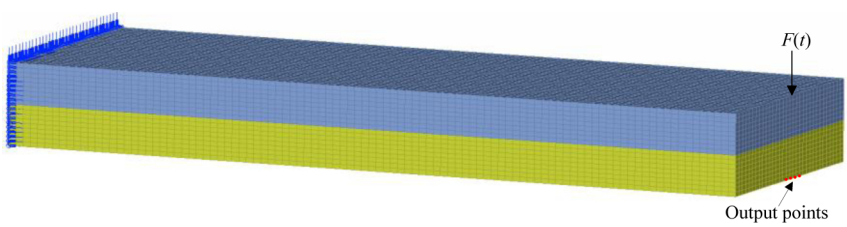

Figure 14. Finite element mesh for the layered cantilever beam model.

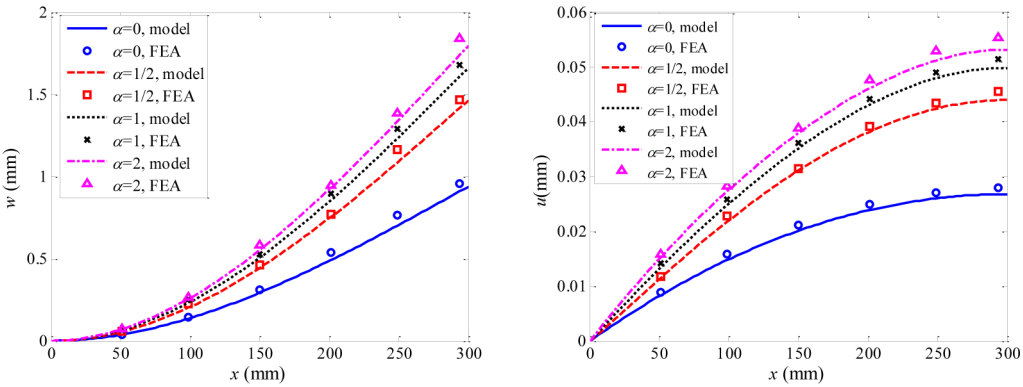

Figure 15. Comparison of vertical deflection and relative slip along the beam length for different pressure distribution laws between theoretical predictions and FEA under normal load F=160N.

distribution laws are calculated using the established FE model. The obtained FEA results are compared with the theoretical model predictions, as shown in Figure 15. It can be seen that the FEA results agree well with the theoretical predictions.

Figure 16 shows examples of the obtained frequency response function (FRF) for the first bending mode of the system under different amplitudes of impulse excitation and different pressure distribution laws. It can be seen that the natural frequency of the system at this mode is f_n=373 Hz. The values of damping ratio are calculated using (25) as $\zeta = 0.033, 0.026, 0.032, 0.024$, respectively.

Figure 17 shows the comparison of damping ratio versus applied normal load between model predictions and FEA results for different pressure distribution laws. It can be seen that that the model predictions agree well with the FEA results, which validates the developed model and the obtained results.

5. Conclusions

In this work, the energy dissipation and the damping capacity of clamped and layered beams under vertical load has been studied using continuum elastic beam model by considering the effect of nonuniform pressure distribution of exponent law. The relative dynamic slip along the contact interface and the associated frictional energy dissipation has been presented. It has been shown that minimum critical vertical loads exist to induce the relative slip along the contact interface. The hysteresis curves at the contact interface have been presented and the damping ratio of the assembled structure has been evaluated. It is shown that peak values of damping ratio exist for different pressure distribution laws and the normal load at which the peak damping ratio occurs is a function of the pressure distribution law. Good agreement between model predictions and three-dimensional finite element analysis validates the developed model and the obtained results. The present study can help to estimate the damping capacity of the layered and jointed structures in order to maximize it as the requirement in real applications. However, the present work is limited to the clamped and layered structures with single interface. Actually, the multilayered composite bolted joints are receiving widespread applications due to their excellent performance high stiffness and strength. Further research is necessary to be conducted on the interfacial slip damping in multilayered bolted structures.

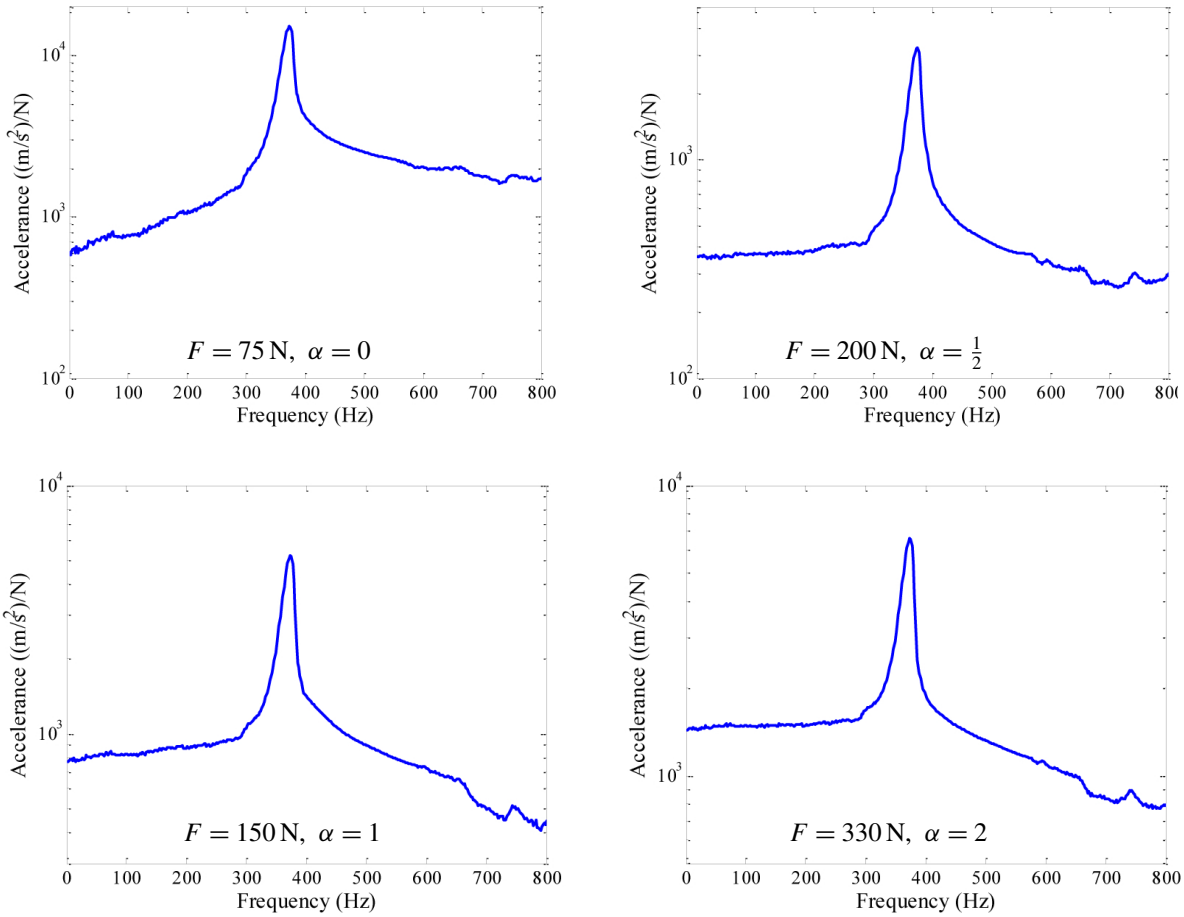

Figure 16. Frequency response function of the system for different amplitudes of impulse excitation and different pressure distribution laws.

Acknowledgement

This work was supported by the National Natural Science Foundation of China, grant number 51775037.

References

[Abad et al. 2014] J. Abad, F. J. Medel, and J. M. Franco, "Determination of Valanis model parameters in a bolted lap joint: Experimental and numerical analyses of frictional dissipation", *Int. J. Mech. Sci.* **89** (2014), 289–298.

[Ahmadian and Jalali 2007] H. Ahmadian and H. Jalali, "Identification of bolted lap joints parameters in assembled structures", *Mech. Syst. Signal Process.* **21** (2007), 1041–1050.

[Asadi et al. 2012] K. Asadi, H. Ahmadian, and H. Jalali, "Micro/macro-slip damping in beams with frictional contact interface", *J. Sound Vib.* **331** (2012), 4704–4712.

[Berger 2002] E. J. Berger, "Friction modelling for dynamic system simulation", *Appl. Mech. Rev.* (*ASME*) **55(6)** (2002), 535–577.

[Chen and Deng 2005] W. Chen and X. Deng, "Structural damping caused by micro-slip along frictional interfaces", *Int. J. Mech. Sci.* **47** (2005), 1191–1211.

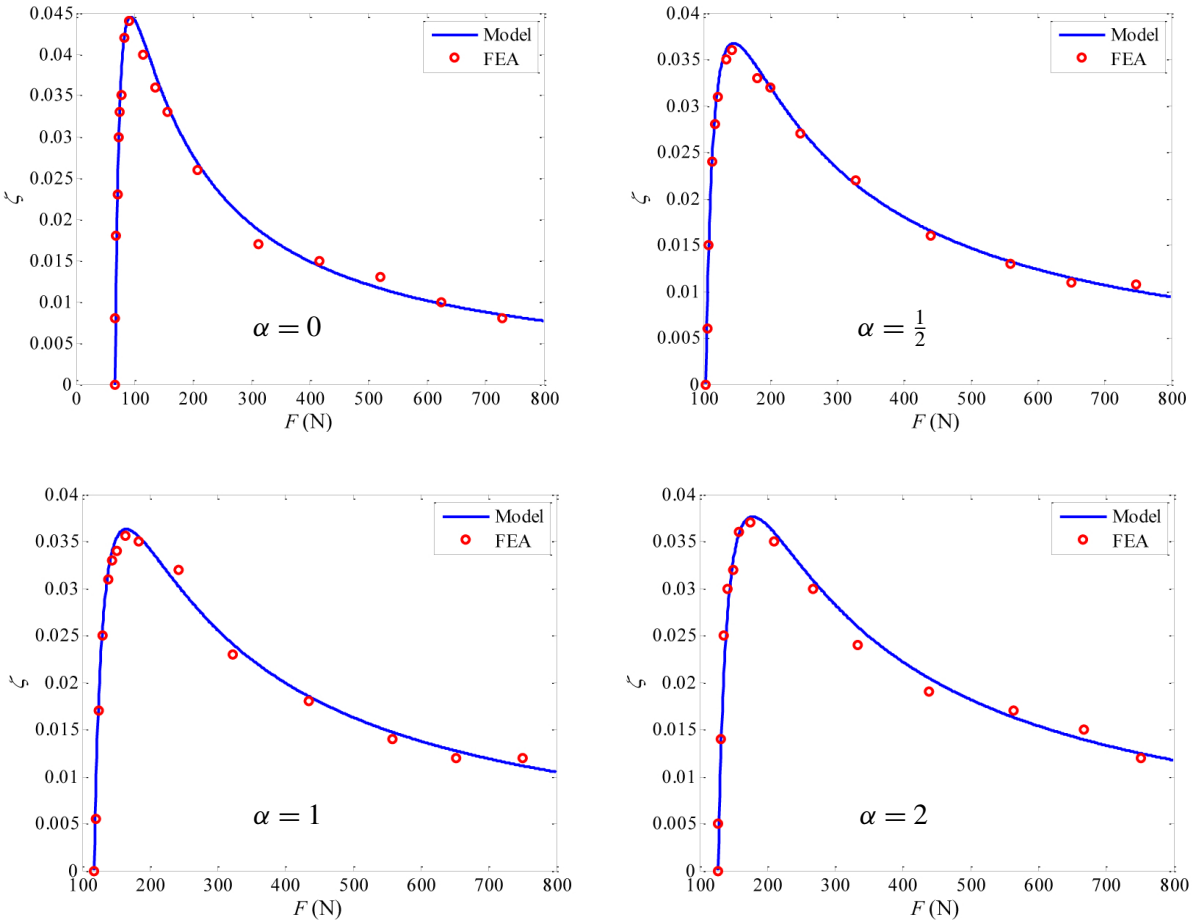

Figure 17. Comparison of damping ratio versus normal load between model predictions and FEA results for different pressure distribution laws.

[Choi et al. 2018] J.-I. Choi, S. M. Hasheminia, H.-J. Chun, J.-C. Park, and H. S. Chang, "Failure load prediction of composite bolted joint with clamping force", *Compos. Struct.* **189** (2018), 247–255.

[Cigeroglu et al. 2006] E. Cigeroglu, W. M. Lu, and C.-H. Menq, "One-dimensional dynamic microslip friction model", *J. Sound Vib.* **292** (2006), 881–898.

[Csaba 1998] G. Csaba, "Forced response analysis in time and frequency domains of a tuned bladed disk with friction dampers", *J. Sound Vib.* **214** (1998), 395–412.

[Daouk et al. 2017] S. Daouk, F. Louf, C. Cluzel, O. Dorival, L. Champaney, and S. Audebert, "Study of the dynamic behavior of a bolted joint under heavy loadings", *J. Sound Vib.* **392** (2017), 307–324.

[Ewins 2000] D. Ewins, *Modal testing: theory*, Practice and Application Research Studies Press Ltd, 2000.

[Gould and Mikic 1972] H. H. Gould and B. B. Mikic, "Areas of contact and pressure distribution in bolted joints", *J. Eng. Industry* (*ASME*) **94**:3 (1972), 864–870.

[Hammami et al. 2016] C. Hammami, E. Balmes, and M. Guskov, "Numerical design and test on an assembled structure of a bolted joint with viscoelastic damping", *Mech. Syst. Signal Process.* **70–71** (2016), 714–724.

[Iwan 1966] W. D. Iwan, "A distributed-element model for hysteresis and its steady-state dynamic response", *J. Appl. Mech.* (*ASME*) **33** (1966), 893–900.

[Li et al. 2017] Y. K. Li, Z. M. Hao, J. Q. Feng, and D. G. Zhang, "Investigation into discretization methods of the six-parameter Iwan model", *Mech. Syst. Signal Process.* **85** (2017), 98–110.

[Marshall et al. 2006] M. B. Marshall, R. Lewis, and R. S. Dwyer-Joyce, "Characterisation of contact pressure distribution in bolted joints", *Strain* **42** (2006), 31–43.

[Masuko et al. 1973] M. Masuko, Y. Ito, and K. Yoshida, "Theoretical analysis for a damping ratio of jointed cantibeam", *Bull. Jpn. Soc. Mech. Eng.* **16** (1973), 1421–1432.

[Menq et al. 1986] C.-H. Menq, J. Bielak, and J. H. Griffin, "The influence of microslip on vibratory response, part I: a new microslip model", *J. Sound Vib.* **107(2)** (1986), 279–293.

[Miller and Quinn 2009] J. D. Miller and D. D. Quinn, "A two-sided interface model for dissipation in structural systems with frictional joints", *J. Sound Vib.* **321** (2009), 201–219.

[Nanda 2006] B. K. Nanda, "Study of the effect of bolt diameter and washer on damping in layered and jointed structures", *J. Sound Vib.* **290** (2006), 1290–1314.

[Segalman 2005] D. J. Segalman, "A four-parameter Iwan model for lap-type joints", *J. Appl. Mech.* (*ASME*) **72** (2005), 752–760.

[Song et al. 2004] Y. Song, C. J. Hartwigsen, D. M. McFarland, A. F. Vakakis, and L. A. Bergman, "Simulation of dynamics of beam structures with bolted joints using adjusted Iwan beam elements", *J. Sound Vib.* **273** (2004), 249–276.

[Stocchi et al. 2013] C. Stocchi, P. Robinson, and S. T. Pinho, "A detailed finite element investigation of composite bolted joints with countersunk fasteners", *Composites A* **52** (2013), 143–150.

[Thai and Uy 2015] H.-T. Thai and B. Uy, "Finite element modeling of blind bolted composite joints", *J. Constr. Steel Res.* **112** (2015), 339–353.

[Xiao et al. 2012] H. F. Xiao, Y. M. Shao, and C. K. Mechefske, "Transmission of vibration and energy through layered and jointed plates subjected to shock excitation", *J. Mech. Eng. Sci.* **226(7)** (2012), 1765–1777.

[Xiao et al. 2014] H. F. Xiao, Y. M. Shao, and J. W. Xu, "Investigation into the energy dissipation of a lap joint using the one-dimensional microslip friction model", *Eur. J. Mech. A Solids* **43** (2014), 1–8.

[Yokoyama et al. 2012] T. Yokoyama, M. Olsson, S. Izumi, and S. Sakai, "Investigation into the self-loosening behavior of bolted joint subjected to rotational loading", *Eng. Failure Anal.* **23** (2012), 35–43.

[Zhong 1993] Z. H. Zhong, *Finite element procedures for contact-impact problems*, Oxford University Press, 1993.

Received 10 Sep 2018. Revised 26 Mar 2019. Accepted 26 Feb 2020.

HUIFANG XIAO: huifangxiao@ustb.edu.cn
, *University of Science and Technology Beijing, Beijing, 100083, China*

YUNYUN SUN: yunyunsunustb@163.com
, *University of Science and Technology Beijing, Beijing, China, China*

JINWU XU: jwxuustb@163.com
, *University of Science and Technology Beijing, Beijing, 100083, China*

JOURNAL OF MECHANICS OF MATERIALS AND STRUCTURES

msp.org/jomms

Founded by Charles R. Steele and Marie-Louise Steele

See msp.org/jomms for submission guidelines.

JoMMS (ISSN 1559-3959) at Mathematical Sciences Publishers, 798 Evans Hall #6840, c/o University of California, Berkeley, CA 94720-3840, is published in 10 issues a year. The subscription price for 2020 is US $660/year for the electronic version, and $830/year (+$60, if shipping outside the US) for print and electronic. Subscriptions, requests for back issues, and changes of address should be sent to MSP.

JoMMS peer-review and production is managed by EditFLOW® from Mathematical Sciences Publishers.

PUBLISHED BY

mathematical sciences publishers

nonprofit scientific publishing

http://msp.org/

Journal of Mechanics of Materials and Structures

Volume 15, No. 3 May 2020